Simulation and Optimization of Vacuum Swing Adsorption Units for Spacesuit Carbon Dioxide and Humidity Control

Michael J. Swickrath* and Molly Anderson †
NASA Johnson Space Center, Houston, TX, 77058
Summer McMillin‡
Engineering and Science Contract Group - Jacobs Technology, Houston, TX, 77058
Craig Broerman§
Engineering and Science Contract Group - Hamilton Sundstrand, Houston, TX, 77058

Controlling carbon dioxide (CO_2) and humidity levels in a spacesuit is critical to ensuring both the safety and comfort of an astronaut during extra-vehicular activity (EVA). Traditionally, this has been accomplished utilizing either non-regenerative lithium hydroxide (LiOH) or regenerative but heavy metal oxide (MetOx) canisters which pose a significant weight burden. Although such technology enables air revitalization, the volume requirements to store the waste canisters as well as the mass to transport multiple units become prohibitive as mission durations increase. Consequently, motivation exists toward developing a fully regenerative technology for spacesuit environmental control.

The application of solid amine materials with vacuum swing adsorption technology has shown the capacity to control CO_2 while concomitantly managing humidity levels through a fully regenerative cycle eliminating constraints imposed with the traditional technologies. Prototype air revitalization units employing this technology have been fabricated in both a rectangular and cylindrical geometry. Experimental results for these test articles have been collected and are described herein. In order to accelerate the developmental efforts, an axially-dispersed plug flow model with an accompanying energy balance has been established and correlated with the experimental data. The experimental and simulation results display good agreement for a variety of flow rates (110-170 ALM), replicated metabolic challenges (100-590 Watts), and atmosphere pressures under consideration for the spacesuit (248 and 760 mm Hg). The testing and model results lend insight into the operational capabilities of these devices as well as the influence the geometry of the device has on performance. In addition, variable metabolic profiles were imposed on the test articles in order to assess the ability of the technology to transition to new metabolic conditions. The advent of the model provides the capacity to apply computer-aided engineering practices to support the ongoing efforts to optimize and mature this technology for future application to space exploration.

I. Introduction

During extra-vehicular activity (EVA), an astronaut inspires oxygen for metabolic activities producing CO_2 and water vapor as byproducts. As CO_2 accumulates, hypercapnia can occur. Alternatively, excess H_2O can condense out of the vapor phase compromising comfort and visibility. Consequently, efficient removal of these compounds is necessary to maintain a safe and comfortable environment within the spacesuit.

*Analyst, Crew and Thermal Systems Division, 2101 NASA Parkway, EC211, Houston, TX, 77058, AIAA Member.
†Analysis Lead, Crew and Thermal Systems Division, 2101 NASA Parkway, EC211, Houston, TX, 77058, AIAA Member.
‡Project Engineer,EVA and Health Systems Group, 2224 Bay Area Blvd., Houston, TX, Member AIAA.
§Project Engineer, CxP and Advanced Systems Group, 2224 Bay Area Blvd., Houston, TX, Member AIAA.

In order to accomplish this task, adsorption has been employed for air revitalization using lithium hydroxide, metal oxides, and zeolites. These adsorbents are either non-regenerable, require significant heat during the regeneration process, heavy and cumbersome to transport, or are highly specific to a single adsorbate.

An alternative approach to removing carbon dioxide and water from the atmosphere includes employing solid amine adsorbents. Such materials have a high affinity for both CO_2 and H_2O and can be readily coated upon a lightweight porous polymer matrix such as polymethyl methacrylate. Moreover, the adsorptive characteristics of these materials enable regeneration through a rapid change in concentration/temperature, or a 'swing', thereby driving the equilibrium to favor adsorbate in the vapor phase. In particular, concentration swings can be achieved through the rapid evacuation of the interstitial gas via exposing the saturated adsorbent to the vacuum of space. Temperature swings can be achieved through contacting adsorbing and desorbing beds in order that the heat evolved through adsorption process is accepted through conduction by the bed undergoing the endothermic desorption process. Utilizing both processes in conjunction has resulted in a thermally-coupled vacuum swing adsorption technology under development by the National Aeronautics and Space Administration (NASA). The interleaved multi-bed solid amine adsorbent technology is comprised of alternating beds that cycle between adsorption and regeneration steps and is referred to as the rapid cycle amine (RCA) and is illustrated in fig 1A.

In a concerted effort to provide lighter mass, smaller volume, increased reliability and robustness, and minimal power, multiple designs remain under aggressive development. Parallel efforts have resulted in two competing RCA designs: a rectangular design (fig. 1B) and a cylindrical design (fig. 1C). In particular, this investigation focuses on the experimental and simulation results for two specific prototypes. The rectangular unit fabricated by Hamilton Sundstrand, referred to in this manuscript as HS-RCA, is a full-scale prototype of the rapid cycle amine relying on a spool valve to direct flow within the unit.[1] Although a number of cylindrical units exist,[2] this manuscript focuses on the experimental and modeling results for the 4-layer sub-scale unit referred to as test article 2 (TA2-RCA). The sub-scale unit TA2-RCA is 4-layers of what is ultimately intended to be a 10-layer unit containing approximately 40% of the proprietary adsorbent SA-9T. To ensure results collected between the two test articles are comparable, flow rates and CO_2 and H_2O injection rates were re-scaled to maintain constant residence times (*i.e.* adsorbent volume divided by flow rate) between the two test articles.

II. RCA Experimental Characterization

The test articles discussed in this manuscript analyzed on the same experimental test stand illustrated in fig. 2. A Reimers Electra AR 68890 boiler system supplies steam to the system. Steam injection was moderated using a regulator to control upstream pressure of a Swagelok micro-metering valve. A Teledyne Hastings HFC-202 mass flow controller was utilized to control CO_2 injection. Nitrogen (N_2) was introduced to the loop as needed to maintain pressure via a check valve. For sub-ambient testing, the loop was depressurized to 4.8 PSIA using a Varian TriScroll 300 vacuum pump. Gas flow within the loop was controlled using a Micronel U51DX-024KK-5 fan which was subsequently measured by a Teledyne Hastings HFM-200 flow meter. Omega Engineering PX177 pressure tranducers reported pressure up and down stream of the test article. Humidity measurement was achieved using Vaisala HMT-334 relative humidity sensors which correlates the electrical properties of a hygroscopic polymer film to ambient water vapor levels. The HMT-334 sensors also recorded temperatures into and out of the bed so that relative humidity can be converted to a concentration or dew point temperature. Carbon dioxide detection was performed with Vaisala GMT/GMP-221 sensors relying non-dispersive infra-red spectroscopy for CO_2 quantification. Once CO_2 and H_2O concentrations were determined from sensor readings, the pressure, temperature, and flow rate data were used to quantify material into and out of the test article. The removal rates, partial pressures, and dew points were subsequently calculated. Additional details regarding the experimental procedures and data analysis have been thoroughly documented elswhere.[3–6]

The metabolic challenges the RCA test articles were subjected to are characteristic to resting (103 W) up to high activity (586 W) and are summarized in table 1. The fan flow rates tested include 113, 127, 142, and 170 actual liters per minute (ALM). These flow rates were chosen as 170 ALM represents the highest achievable flow rate that could be maintained for prolonged periods for the portable life support system (PLSS) fan while the 113 ALM is the lowest flow rate capable of maintaining the accumulated concentration of CO_2 in the spacesuit helmet below a critical threshold through washout. For the sub-scale test article, the fan flow rates and the injection rates summarized in table 1 were re-scaled to 40% of nominal values in

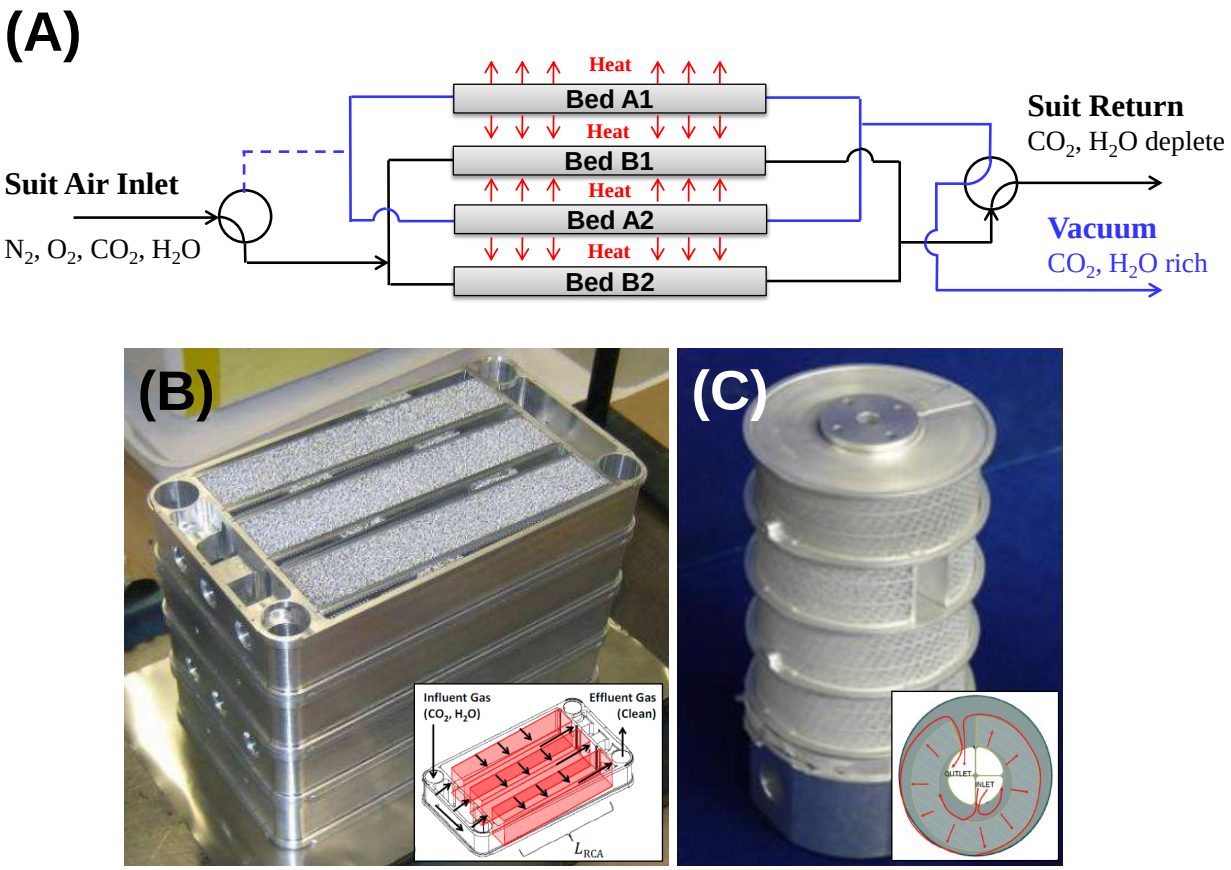

Figure 1. (A) Illustration of RCA operation and flow direction for the (B) full-scale rectangular RCA and the (C) sub-scale cylindrical RCA test articles. The illustration in (A) represents operation with the 'A' beds undergoing vacuum regeneration and 'B' beds undergoing adsorption.

order to maintain equivalent test article residence times. Current requirements for the maximum inhaled CO_2 concentration are established at 7.6 mm Hg for metabolic rates up to 469 Watts (1600 Btu/hr) and 15 mm Hg for metabolic rates exceeding 469 Watts.[1,7] As has been performed in previous analyses,[1,7] the valve(s) diverting flow between adsorbing and desorbing layers was actuated at an outlet partial pressure of 6.0 mm Hg of CO_2. This value was chosen as it provides an extra buffer to ensure the critical concentration is not reached while the volume of accumulated CO_2 is washed out of the test loop following valve actuation. Vacuum regeneration was performed through a variety of scenarios: (1) a vacuum was pulled on both the inlet/outlet of the RCA simultaneously in the dual-end desorb (DEV) configuration, (2) vacuum was pulled on the inlet of the device in the single-end vacuum inlet (SEV-I) configuration, or (3) vacuum was pulled on the outlet of the device in the single-end vacuum inlet (SEV-O) configuration.

III. RCA Predictive Model

A predictive model for the RCA test articles and associated test loop (fig. 2) has been generated and is summarized in table 2. In order to establish this model, a few broad assumptions were employed.

1. Cross-sectional variations in gas temperature, pressure, concentration are negligible. Conversely, variations in the flow direction are significant. As a result, one-dimensional plug flow with axial dispersion becomes a suitable approximation for component material balances, eq. 1.

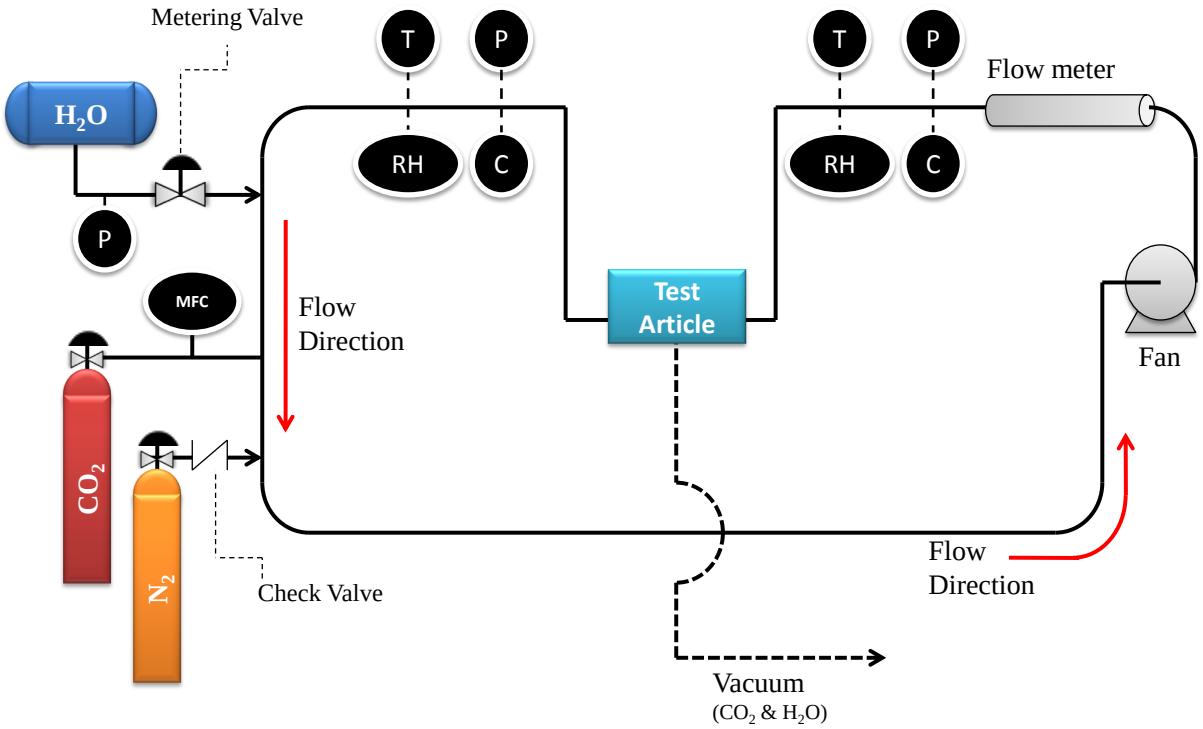

Figure 2. Rapid cycle amine test loop. T: temperature sensor, P: pressure transducer, RH: relative humidity sensor, C: carbon dioxide sensor, MFC: mass flow controller.

2. At the temperatures and pressures explored in this investigation, all gases behave according to the ideal gas equation of state, eq. 2.

3. Pressure drop throughout an adsorbent bed can be approximated utilizing the Blake-Kozeny relationship. The Blake-Kozeny relationship is linear with velocity. However, due to superficial velocity variations as the cross-sectional area changes in the cylindrical unit, a non-linear pressure profile can develop within the cylindrical bed, eq. 3.

4. The rate of adsorption can be adequately described via a linear driving force potential, eq. 4. This expression is exact when mass transfer is controlling or a linear isotherm is used. Otherwise, this relationship generally provides a suitable approximation for non-linear isotherms.[8]

5. Gas and solid phases are in thermal equilibrium. In addition, the bulk density of the solid phase is presumed to be independent of temperature. Consequently, a single energy balance can be employed rather than treating the solid and gas phases independently, eq. 5.

6. Adsorption of CO_2 is described by the Toth isotherm, eq. 6. The Toth isotherm is attractive as (A) it implies a chemisorptive monolayer adsorption mechanism which can be derived from first principles, (B) the Toth isotherm captures linear behavior at low pressures, and (C) the Toth isotherm can account for inhomogeneity of a surface.[9] An additional term, $r_\circ$, has been added to the parameter t in an effort to capture cooperative adsorption between H_2O and CO_2.

7. Adsorption of H_2O is described via a Freundlich isotherm, eq. 7. Limited experimental data for SA9T suggests water adsorbs according to a Type III sorption process.[10] In addition, the water isotherm can be collapsed onto a single curve via re-casting the isotherm into a relative humidity basis simplifying the analyses described herein.

8. A linear profile in gas flow rate has been assumed for all steps, eq. 8. This approach has been suggested by Cruz et al.[11] and has a history of implementation in vacuum swing adsorption modeling.[12] In order

Table 1. Full-scale injection rates employed to simulate metabolic challenge to the RCA test articles in this investigation.

Metabolic Rate, Watts	CO_2 Injection Rate, SLM	H_2O Injection Rate, g/min.
103	0.271	0.60
152	0.402	1.02
249	0.658	1.13
293	0.774	1.44
366	0.967	1.59
469	1.238	1.36
586	1.548	1.29

to determine boundary velocities during vacuum swings, valve equations were employed, eq. 9 and eq. 10.

Parameters for the model described in table 2 are summarized in table 3. Mass, heat, and dispersion coefficients were approximated according to heuristic relationships summarized elsewhere[8] and further optimized against experimental performance data. Isotherm parameters were determined from experimental data relating adsorbent loading to adsorbate concentration. Gas viscosity and heat capacity could either be determined from heuristic relationships reported elsewhere[13] or through internal algorithms in the simulation software used to approximate a solution.

The coupled system of partial differential equations was solved using finite difference techniques through the Aspen Custom Modeler software package. A second order central finite differencing scheme was applied in order to accurately model bi-directional flow that occurs during vacuum desorb. The Gear formulae were used for numerical integration as a result of the ability of the Gear formulae to simulate phenomena with dynamics on drastically different time-scales. The calculations were performed on a CPU with a 2.66 GHz Intel® Core™2 Quad processor and 3.25 GB of RAM. For any specified metabolic rate, pressure, and flow rate, solution generally take several minutes to an hour.

IV. Results & Discussion

In order to maintain a safe environment within the PLSS during extra-vehiclar activity, the rapid cycle amine system is under aggressive developmental efforts for air revitalization. The process is achieved through cycling an interleaved system of thermally-coupled vacuum swing adsorption (VSA) reactors. This concept has been translated into a handful of function prototypes. The prototypes can be classified into either rectangular or cylindrical units. This manuscripts details the experimental results and the results of a correlated model for two such units. With respect to the model, the major difference is attributed to the ∇ operator which assumes different forms for either rectangular (*i.e.* Cartesian) or cylindrical geometry. In addition, the rectangular adsorbent layers maintain a constant cross-sectional area while the cylindrical devices has a change in cross-sectional area as gas flows from the inner to the outer radius. However, before considering the experimental results, it is worth exploring the sorption behavior of carbon dioxide and water on SA9T to develop intuition about the physics through which the RCA works.

A. Sorption Behavior of SA9T

An example solution for these equations is provided in fig. 3. It becomes immediately apparent that the sorption behavior of H_2O and CO_2 are significantly different. The experimental loading data collected for this analysis, along with the magnitude of the heats of adsorption, indicate that water undergoes type III adsorption while CO_2 follows a type I process. In particular, type-I processes are generally represented as a Langmuir process where adsorbate molecules compete for surface sites in which non-covalent interactions result in molecules associating with a surface.[10,14,15] Conversely, type-III processes demonstrate limited sorption at low concentrations followed by an exponential rise in sorption with increasing concentration.

Table 2. Equations for vacuum swing adsorption model.

Component material balance for i as CO_2 or H_2O

$$\epsilon \frac{\partial C_i}{\partial t} + \rho_s \frac{\partial q_i}{\partial t} + \nabla \cdot (\vec{v} C_i) - D_L \nabla^2 C_i = 0 \tag{1}$$

Component balance for N_2 through ideal gas equation of state

$$C_{\mathrm{N_2}} = \frac{P}{R_g T} - C_{\mathrm{CO_2}} - C_{\mathrm{H_2O}} \tag{2}$$

Blake-Kozeny pressure flow relationship

$$-\frac{dP}{dx} = \frac{150 \mu v (1-\epsilon)^2}{D_p^2 \epsilon^3} \tag{3}$$

Linear driving force gas-to-solid mass transfer

$$\rho_s \frac{\partial q_i}{\partial t} = k_i' \left(C_i - C_i^*\right) \tag{4}$$

Energy balance within a bed layer

$$\rho_s c_{p,s} \frac{\partial T}{\partial t} + \epsilon c_{p,g} C \nabla(\vec{v} \cdot T) - K \nabla^2 T + h_{w,g} \left(T - T_{w,u}\right) + h_{w,g} \left(T - T_{w,l}\right) = \rho_s \sum_i E_i \frac{\partial q_i}{\partial t} \tag{5}$$

CO_2 adsorption – Type I Toth isotherm representation

$$q_{co_2} = \frac{a C_{co_2}^*}{\left[1 + \left(b C_{co_2}^*\right)^{1/t}\right]^t} \qquad a = a_\circ \exp\left(\frac{E_{co_2}}{R_e T}\right) \qquad b = b_\circ \exp\left(\frac{E_{co_2}}{R_e T}\right) \qquad t = t_\circ + \frac{c_\circ}{T} + r_\circ RH \tag{6}$$

H_2O adsorption – Type III Freundlich isotherm representation

$$q_{H_2O} = \alpha RH^2 \tag{7}$$

Superficial gas velocity within bed layer

$$Q = Q_f \left(\frac{x}{x_f}\right) + Q_\circ \left(\frac{x_f - x}{x_f}\right) \tag{8}$$

Superficial gas velocity at layer boundaries during vacuum desorption (for P_i in atm and T in K)

If $\frac{P_d}{P_u} < \left(\frac{2}{k+1}\right)^{k/(k-1)}$ flow is choked. $v_{x_o}, v_{x_f}\,[\mathrm{m/s}] = \frac{235.116 C_v P_u}{A_{cs}} \left[\frac{1}{\mathrm{SG} \cdot T}\right]^{1/2}$ (9)

If $\frac{P_d}{P_u} \geq \left(\frac{2}{k+1}\right)^{k/(k-1)}$ flow is not choked. $v_{x_o}, v_{x_f}\,[\mathrm{m/s}] = \frac{277.236 C_v}{A_{cs}} \left[\frac{P_u^2 - P_d^2}{\mathrm{SG} \cdot T}\right]^{1/2}$ (10)

Table 3. Model parameters employed in the simulation of the vacuum swing adsorption process.

Parameter	Value	Dimensions	Description
ρ_s	636.7	kJ/m^3	Actual sorbent density
ϵ	0.343	unitless	Void fraction
D_L	2.90 $\times 10^{-3}$	m^2/s	Dispersion coefficient
k'_{CO_2}	0.735	1/s	Mass transfer coefficient, CO_2
k'_{H_2O}	0.996	1/s	Mass transfer coefficient, H_2O
C_v	1.0	unitless	Valve coefficient
k	1.4	unitless	Isentropic expansion factor
$h_{w,g}$	2.67	kJ/(m^2·s·K)	Wall heat transfer coefficient
K	6.94 $\times 10^{-3}$	kJ/(m·s·K)	Layer thermal conductivity
$C_{p,s}$	2.04	kJ/(kg · K)	SA9T specific heat
E_{CO_2}	94.0	kJ/mole·K	Isoteric heat of adsorption, CO_2
E_{H_2O}	44.0	kJ/mole·K	Isoteric heat of adsorption, H_2O
a_o	1.312×10^{-15}	m^3/kg SA9T	CO_2 Toth isotherm parameter
b_o	7.350×10^{-13}	m^3/kmole CO_2	CO_2 Toth isotherm parameter
c_o	93.748	K	CO_2 Toth isotherm parameter
r_o	0.193	unitless	CO_2 Toth isotherm parameter
t_o	7.350	unitless	CO_2 Toth isotherm parameter
α	0.0164	unitless	H_2O Freundlich isotherm parameter

This is related to non-covalent interaction amongst adsorbate molecules. In this situation, the following mechanism is presumed. At low concentrations, a limited but sufficient amount of water adsorbs to the SA9T. The decreased affinity for SA9T is seen in the isotherm as well as in the isoteric heat adsorption indicating bonding is weaker for H_2O than for CO_2. As loading increases, greater amounts of water adsorb and the adsorbed water begins to hydrogen bond with water in the vapor phase. This process leads to the exponential relationship between concentration and loading for water.

To explore the implications of this process, the model was employed to generate breakthrough curves for SA9T according to the isotherm data. For this experiment, a single flow stream into the RCA was modeled with a flow rate of 170 ALM, a pressure of 14.7 PSIA, the CO_2 partial pressure of the stream was 5.0 mm Hg, and water content resulted in a dew point of 44.6 °F. The results of this experiment are shown in fig. 3. As demonstrated in fig. 3, CO_2 systematically loads from the front of the bed through the back of the bed. This is the typical breakthrough curve one would expect for a Langmuir type process.[16] Over the course of the 60 minute theoretical experiment, very little carbon dioxide would be observed to leave the bed until around 50 minutes into the experiment. In contrast, water very quickly is transported through the bed in low concentrations. In this situation, water would be observed the leave the bed almost instantly. As time progresses the concentration within the bed would build while outlet dew point would also be observed to increase. The loading results (fig. 3) demonstrate a similar trend. Carbon dioxide loads from front-to-back over time while water begins loading over the entire interior of the bed at the outset of the experiment. It is through these mechanisms that the salient features of the dew point and CO_2 partial pressure profiles versus time arise.

B. Half-cycle Results

Fig. 5 demonstrates experimental and model results for ambient testing at 170 ALM equivalent for the sub-scale cylindrical test article with a metabolic challenge of 366 Watts (1250 Btu/hr). The profiles exhibited in this figure were typical of what was observed for all experimental data. As indicated in the figure, the time requirement until the valve cycles agrees favorably between the model and experiment. Furthermore, for the metabolically imposed injection rate of H_2O, the inlet and outlet dew points correspond with one another well. The model predicts a mean outlet dew point of 16.5 °F while the experimental measurement was 18.1 °F. In

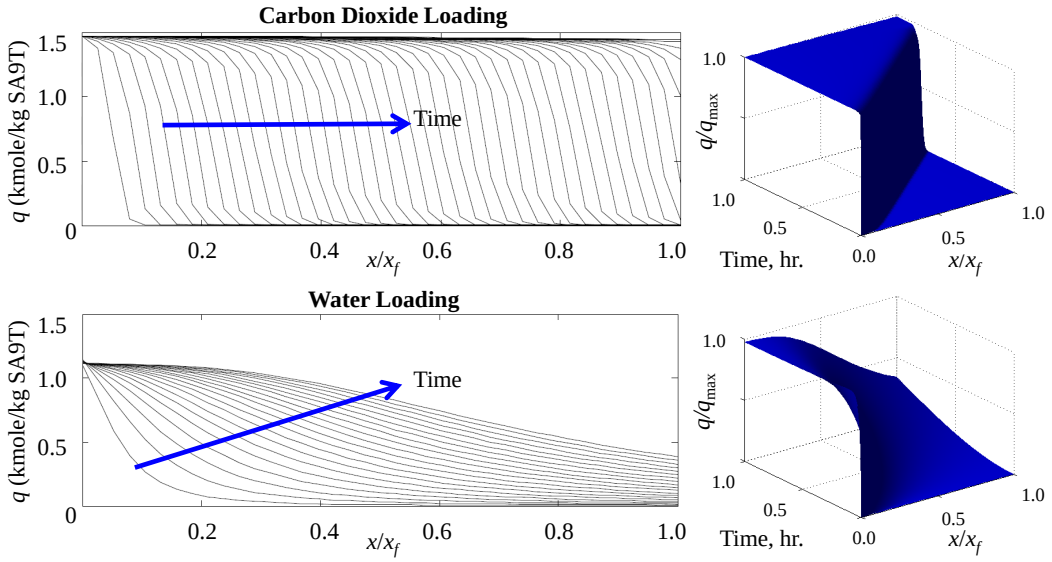

Figure 3. SA9T loading curves and surfaces for CO_2 and H_2O . Inlet flow conditions: flow rate = 170 ALM, P = 14.7 PSIA, P_{co_2} = 5.0 mm Hg, T_d = 44.6 °F.

comparison, the experimental versus model carbon dioxide results demonstrate decent agreement although the experimental data demonstrates a peculiar trend. The smoothed profiles of the experimental results demonstrate an internal time-averaging algorithm performed by the Vaisala GMP/GMT-221 CarboCap® sensors employed to minimize experimental noise in the reported signal. Conversely, the deterministic model is devoid of noise and has no need for a data smoothing. In spite of the smoothing algorithm, both the experimental and simulation results predict comparable time to half-cycle which indicates how quickly the adsorbent material within the RCA saturates.

C. Half-cycle Time for Various Configurations

As mentioned above, as a means of feedback control to ensure efficient operation, the valve(s) determining which bed experiences adsorption versus desorption are actuated if the outlet concentration reaches 6.0 mm Hg. During a valve cycling event, the adsorbing and desorbing beds equalize to 7.35 PSIA. Following equalization, the previously adsorbing bed enters desorption dumping the interstitial volume to vacuum. This is associated with a loss in gas commodities.

Physically, this is the time requirement to saturate the bed to the point to breakthrough and the outlet concentration reaches this threshold. This is associated with the formation of a carbon dioxide monolayer on the adsorbent exhausting all available bonds. The amount of material required to achieve saturation can be determined *a priori* from the Toth isotherm. Taking the limit as $C^*_{co_2} \rightarrow \infty$, the saturation capacity of SA9T becomes a/b pertaining to 1.78 moles CO_2/kg SA9T. Consequently, the time requirement to reach an outlet condition of 6.0 mm Hg is dependent upon injection rate rather than the flow rate. Through this process, all flow rate curves collapse to a single curve. In addition, at cyclic-steady state, the conductance to vacuum and heat transfer capabilities determine how much regeneration can occur during desorption also influence half-cycle time. Consequently, additional approaches to optimization may include maximizing half-cycle time through decreased test article pressure drop characteristics or improved heat transfer capabilities.

As a result of these factors, the half-cycle time was meticulously monitored as an indicator of performance. Shorter half-cycle times for identical test conditions are perceived as a more favorable characteristic. These results are summarized in fig. {fig:DEVAmb1 indicating the mean time to half-cycle for all fan flow rates versus test article and desorb scenario. For all data collected, the model and experimental results demonstrate excellent agreement. For the cylindrical unit TA2, SEV-I had the shortest half-cycles followed by a marginal increase in half-cycle time for SEV-O and then DEV. This observation seems plausible as DEV desorb would have much less intra-bed resistance since two orifices exist through which interstitial gas can leave.

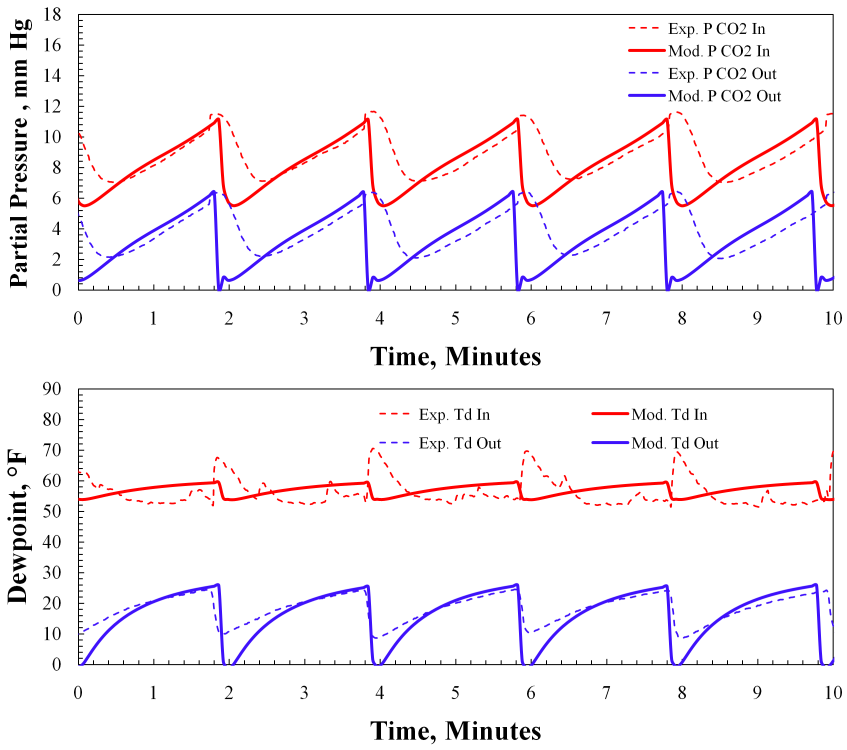

Figure 4. Ambient DEV results at the sub-half-cycle scale for 366 Watt (1250 Btu/hr) at 170 ALM. (Top) Partial pressure of CO_2 and (Bottom) dew point into and out of the RCA.

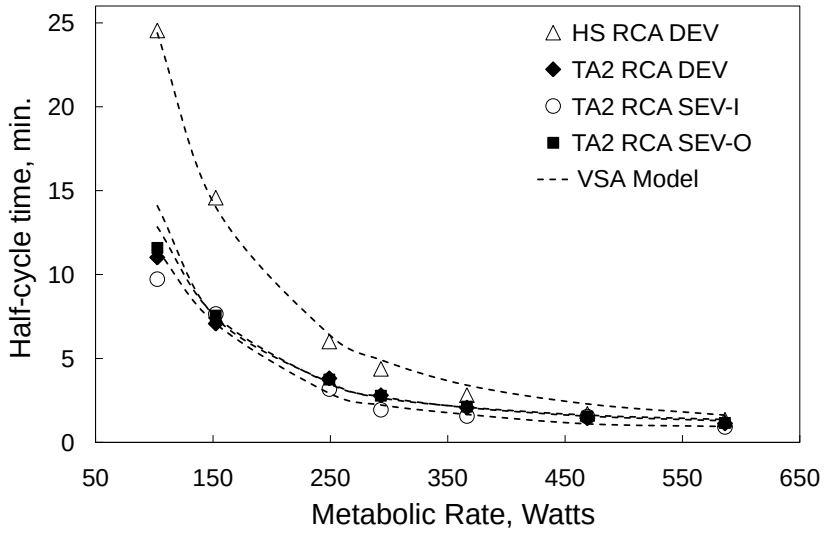

Figure 5. Mean time to half-cycle for all flow rates for each test article with multiple desorption configurations.

Moreover, the HS-RCA demonstrated a significantly higher time to half-cycle than did TA2-RCA unit. Care must be taken to infer the right conclusion from this result. This may mean the rectangular unit was designed better with an decreased test article pressure drop and/or better heat rejection capabilities. Conversely, this could be an artifact the configuration of the test loop. Specifically, HS-RCA has an engineered spool valve properly directing the flow through the test article. In contrast, TA2-RCA currently does not

currently have a valve and an *ad hoc* valving system was built from solenoid valves for this phase of testing. This decreased half-cycle time could be associated a significant increase in pressure drop through the solenoid valving system. Although the explanation is currently unclear, the correlated model has demonstrated the capacity to generate valid half-cycle time predictions for these test articles. As a result, the model might provide the key to determining whether the test article geometry significantly influences the performance of the RCA vacuum swing adsorption system. These results will be discussed in the latter portion of this manuscript.

D. Variable Metabolic Challenge

Although knowing the performance of the RCA unit during cyclic steady-state is insightful toward understanding the capabilities of this technology; during extra-vehicular activity, the unit will most likely be subject to multiple metabolic rates that may change at a frequency in which cyclic steady-state is not achieved. As a result, tests were performed to characterize the performance of the RCA unit under non-steady state operation. In particular, two variable metabolic rate experiments were considered. Both a 7 hour and an 8 hour metabolic simulations were designed to mimic the variable profile of an astronaut performing the respective duration of extra-vehicular activity (EVA). These experiments were designed to (A) establish whether or not the RCA unit could effectively mitigate carbon dioxide levels under non-cyclic steady state conditions and (B) to understand how quickly the RCA unit can transition between intermediate steady-state conditions to new constraints on the system. Although both 7 and 8 hour profiles were collected for 110 and 170 ALM flow rates for the rectangular HS-RCA, the results presented herein will focus on the 110 ALM 8 hour results. The other results not explicitly depicted in this report follow similar trends to those included below and can be found elsewhere for the intrigued reader.[5] The 8-hour variable metabolic profile imposed on the test article is summarized in table 4.

Table 4. 8-hour variable metabolic profile experiment for the HS-RCA.

Sequence [No.]	Met. Rate [Watts]	Flow Rate [ALM]	CO_2 Injection [SLM]	Dew Point [°F]	Duration [min.]
1	249	110	0.658	51.0	30
2	322	110	0.851	51.0	60
3	601	110	1.586	51.0	10
4	100	110	0.263	51.0	50
5	334	110	0.882	51.0	60
6	469	110	1.238	51.0	30
7	249	110	0.658	51.0	30
8	322	110	0.851	51.0	60
9	601	110	1.586	51.0	10
10	100	110	0.263	51.0	44
11	334	110	0.882	51.0	81
11	469	110	1.238	51.0	15

The results for the variable profile investigation are displayed in fig. 6. Both the experimental and simulation results demonstrate the HS-RCA was capable of handling the metabolic challenge of the simulated 8-hour extra-vehicular activity. The higher metabolic rates forced the RCA to cycle more quickly in order to maintain CO_2 concentration below the critical threshold. The shorter half-cycles were also associated with a decrease in the dew point. The model predicts comparable half-cycle times as were recorded experimentally although the inlet CO_2 flow rates was somewhat lower in the model than recorded experimentally. With regard to dew point, both the model and experiment show that as half-cycle time is increased, water accumulates in the system leading to higher dew points. This trend reverses for the higher metabolic rates where the RCA valve cycles faster. Overall, these results are encouraging as they indicate that the RCA technology should be capable of handling a wide variety of metabolic rates and should also be capable of transitioning quickly between states as activity is either increased or decreased.

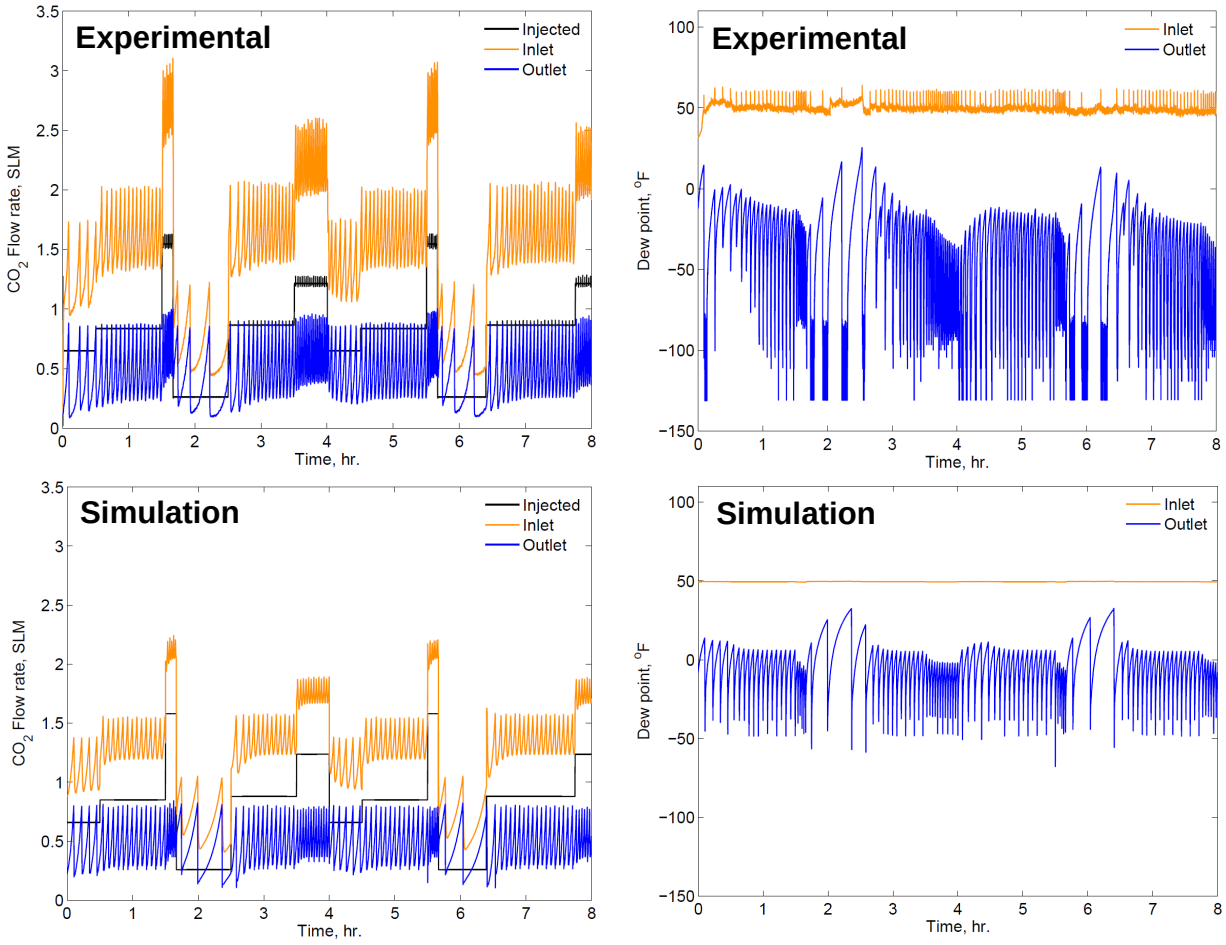

Figure 6. 8-hour variable metabolic profile experimental (top panel) and simulation (bottom panel) results for a 110 ALM flow rate.

E. Geometrical Considerations in VSA System Design

The experiments to date have resulted in the generation of a copious amount of data to characterize the performance of both rectangular and cylindrical RCA designs. It is the goal of these exercises to determine whether the geometry can significantly influence performance. A direct comparison of the data collected is not exactly possible for a two primary reasons.

(1) The rectangular and cylindrical test articles had drastically different valving systems. The rectangular unit has a spool valve which could be plumbed to the vacuum chamber with relative ease. Currently, the cylindrical test article did not have a dedicated valve but instead relied upon a series of 8 solenoid valves to direct flow. The solenoid valves required a decrease in tubing diameter from the vacuum chamber to the test articles to interface with the RCA unit. Additionally, the solenoid valves resulted in plumbing that had several bifurcations between the vacuum chamber and test article. Consequently, the pressure drop between the vacuum chamber and test articles was not equivalent for both series of tests and may have influenced the results.

(2) The interior design of both test articles (*i.e.* flow manifolds and plenums) presumably result in significantly different pressure drop throughout the competing geometries. Although the pressure drop through the porous media was considered in the development of the 1D predictive models, the models currently lack the sophistication required to effectively analyze 3D pressure variations within the ullage volume of the RCA units and the associated influence this might have on vacuum desorb performance.

Consequently, these factors may have served to confound the results rendering a direct comparison difficult. Alternatively, a predictive model has been generated and correlated to experimental data for both

the cylindrical and rectangular RCA designs. Consequently, conductance to vacuum, and all other factors, can be held constant within the model in order to gain insight about how the device geometry influences performance.

This analysis was performed for both the cylindrical and rectangular geometries. In this analysis, dual-end vacuum was considered for desorption since experimental data existed for both test articles for correlation of the DEV model. The flow rate was set to 170 ALM while all metabolic profiles were explored as summarized by table 1. The conductance to vacuum for the model was more closely associated with the conductance for the cylindrical test article and associated solenoid valving. This was chosen as the basis for comparison as the cylindrical system ostensibly has increased pressure drop and serves as a more conservative estimate of RCA capabilities.

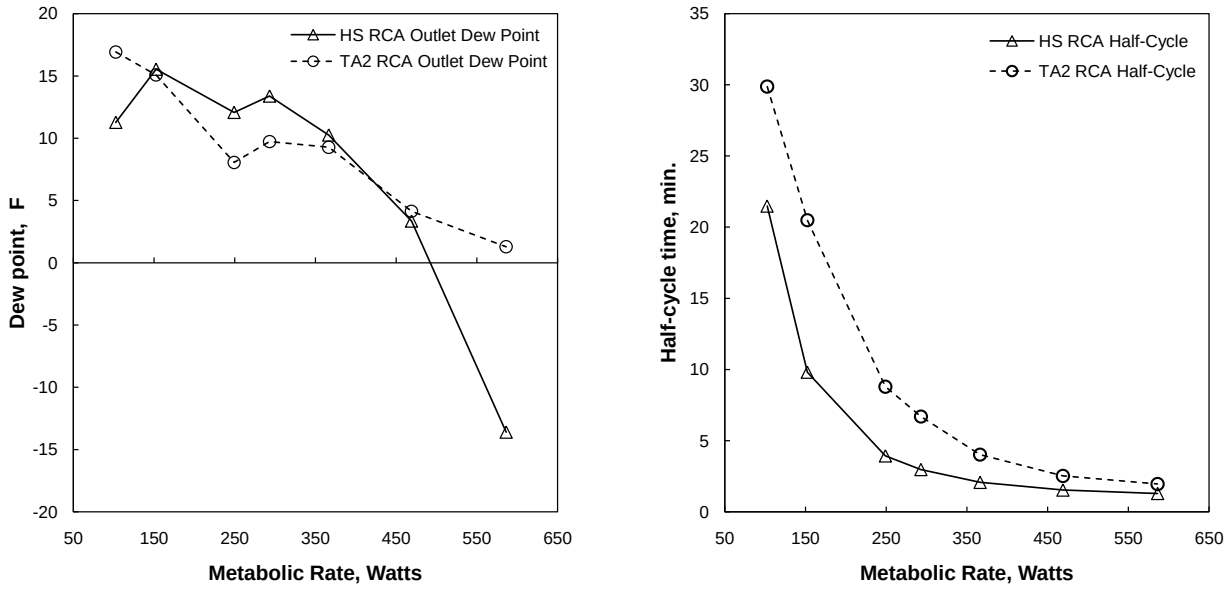

Figure 7. Simulation results for rectangular versus cylindrical designs with comparable vacuum conductance in dual-end vacuum desorb mode.

The results for this analysis are depicted in fig. 7. The results demonstrate that the cylindrical geometry provides a slightly longer half cycle time than the rectangular unit. This result can be explained through considering the geometry. Since both theoretical units experience equal conductance to vacuum and the same starting pressure, the inlet side of both units will have similar de-pressurization profiles as they desorption occurs. Conversely, the cross sectional area of the cylindrical unit decreases radially while the rectangular has a constant cross-section. The increase in cross-section of the cylindrical unit results in a decrease in superficial velocity, and thereby pressure drop, to the outlet side improving the ability to de-pressurize and desorb from the back side of the cylindrical unit. This results in increased half-cycle time. With regard to mean outlet dew point, the cylindrical unit tends to have outlet dew points within a smaller band than the rectangular unit. This result is associated with the disparity in half-cycle times between the two units. For the cylindrical unit with the longer half-cycle time, the bed achieves a more loaded cyclic state. As a result, outlet dew points tend to be higher driving the mean outlet dew point to a higher value than the rectangular unit. These results suggest there could be a performance advantage for the cylindrical design pending pressure drop associated with valves, manifolds, and plenums are kept equal. However, the caveat may present a challenge a the cylindrical unit my need to consist of several more layers than a rectangular unit to maintain a small device diameter. This would presumably increase the pressure drop within the test article and will be investigated in future performance testing.

V. Conclusions

The results presented within this manuscript summarizes the development of a model for the rapid cycle amine technology from first principles. The model has been correlated against experimental data with good agreement for a variety of desorption modes. In addition, good agreement was also established for an eight hour variable metabolic profile challenge to the RCA.

Moreover, a theoretical investigation was performed to assess whether the geometry alone significantly influences performance when conductance to vacuum is equivalent for the competing designs. This experiment was prohibited as the prototype units had different valving systems and plenum geometries that serve to impose varying levels of resistance to the system. The theoretical investigation suggests that the cylindrical unit operated in dual-end vacuum desorb mode could lead to increased half-cycle times than the rectangular unit. If achieved in practice, this would result in less ullage gas losses during EVA. However, this theoretical result is strongly tied to the device design and will ultimately need to be revisited as designs are optimized.

References

[1]Papale, W., Paul, H., and Thomas, G., "Development of Pressure Swing Adsorption Technology for Spacesuit Carbon Dioxide and Humidity Removal," *Proceedings of the International Conference on Environmental Systems*, SAE International, Norfolk, VA, 2006, Paper No. 2006-01-2203.

[2]Hanford, A. and Pinckney, J., "Summary of Testing to Date for the Rapid Cycle Amine Test Articles," Tech. Rep. ESCG-4470-09-TEAN-DOC-0105-A, Engineering and Science Contract Group, Houston, TX, August 2009.

[3]McMillin, S., "Engineering Science Contract Group Test Article 2 Rapid Cycle Amine (RCA) Carbon Dioxide And Humidity Removal System Test Report," Tech. Rep. ESCG-4245-10-EVAHS-DOC-0084, Engineering and Science Contract Group, Houston, TX, September 2010.

[4]McMillin, S., "Hamilton Sundstrand Rapid Cycle Amine (RCA) Carbon Dioxide and Humidity Removal System Test Report," Tech. Rep. ESCG-4245-10-EVAHS-DOC-0006, Engineering and Science Contract Group, Houston, TX, May 2010.

[5]Swickrath, M., "Hamilton Sundstrand Rapid Cycle Amine (RCA) Carbon Dioxide and Humidity Removal System Analysis Report," Tech. Rep. ESCG-4470-10-TEAN-DOC-0077, Engineering and Science Contract Group, Houston, TX, June 2010.

[6]Swickrath, M., "Test Article 2 Rapid Cycle Amine Carbon Dioxide and Humidity Removal System Analysis Report," Tech. Rep. CTSD-ADV-875, National Aeronautics and Space Administration, Johnson Space Center, Houston, TX, January 2011.

[7]Seter, A., "Allowable Exposure Limits for Carbon Dioxide During Extravehicular Activity," Tech. Rep. 103832, National Aeronautics and Space Administration, April 1993.

[8]LeVan, M., Carta, G., and Yon, M., "Chap. 16: Adsorption and Ion Exchange," *Perry's chemical engineers' handbook*, McGraw-Hill New York, 7th ed., 1997.

[9]Wang, Y. and LeVan, M., "Adsorption Equilibrium of Carbon Dioxide and Water Vapor on Zeolites 5A and 13X and Silica Gel: Pure Components," *Journal of Chemical & Engineering Data*, Vol. 54, No. 10, 2009, pp. 2839–2844.

[10]Adamson, A. and Gast, *Physical chemistry of surfaces*, Wiley, New York, 1997.

[11]Cruz, P., Santos, J., Magalhaes, F., and Mendes, A., "Simulation of separation processes using finite volume method," *Computers & chemical engineering*, Vol. 30, No. 1, 2005, pp. 83–98.

[12]Agarwal, A., Biegler, L., and Zitney, S., "Simulation and optimization of pressure swing adsorption systems using reduced-order modeling," *Industrial & Engineering Chemistry Research*, Vol. 48, No. 5, 2008, pp. 2327–2343.

[13]Sandler, S., *Chemical and engineering thermodynamics*, John Wiley & Sons, 1989.

[14]Fogler, H., Vennema, A., and Vennema, C., *Elements of chemical reaction engineering*, Prentice-Hall Englewood Cliffs, NJ, 1992.

[15]Rawlings, J. and Ekerdt, J., *Chemical reactor analysis and design fundamentals*, Nob Hill Publishing, Madison, WI, 2002.

[16]Geankoplis, C., *Transport processes and separation process principles (includes unit operations)*, Prentice Hall Press Upper Saddle River, NJ, USA, 2003.

Nomenclature

Acronyms

ACFM	Absolute cubic feet per minute
Btu	British thermal unit
CO_2	Carbon dioxide
DEV	Dual-end vacuum regeneration
EVA	Extra-vehicular activity
H_2O	Water

LiOH	Lithium hydroxide
MetOx	Metal oxide
PLSS	Portable life support system
PSIA	Pounds per square inch (absolute)
RCA	Rapid cycle amine
SA9T	Hamilton Sundstrand proprietary solid amine sorbent formulation
SEV-I	Single-end vacuum generation on inlet side
SEV-O	Single-end vacuum generation on outlet side
SLM	Standard liters per minute
TA2	Test article 2
VSA	Vacuum swing adsorption

Variables

a,a_o	Parameters for Toth isotherm, [m^3/kg SA9T]
A_{cs}	Cross-sectional area, [m^2]
b,b_o	Parameters for Toth isotherm, [m^3/kmole]
c_o	Parameters for Toth isotherm, [K]
C_{gas}	Overall gas concentration (sum of component concentrations), [kmole/m^3]
C_i	Concentration of component i, [kmole/m^3]
C_i^*	Concentration of component i at equilibrium, [kmole/m^3]
$C_{p,i}$	Specific heat of component i, [kJ/(kmole·K)]
C_v	Valve coefficient, [unitless]
D_p	Mean particle diameter of sorbent beads, [m]
D_L	Dispersion coefficient, [m^2/s]
E_i	Isoteric heat of adsorption for component i, [kJ/kmole]
$h_{w,g}$	Heat transfer coefficient for wall-gas, [kJ/(m^2·s·K)]
K	Thermal conductivity, [kJ/(m·s·K)]
k	Isentropic expansion factor, [unitless]
k_i'	Mass transfer coefficient of component i, [1/s]
m_i	Mass flow rate of component i, [kg/min.]
Mw_i	Molecular weight of component i, [kg/kmole]
N_i	Moles of component i, [kmole]
P	Pressure, [PSIA] -or- [bar]
P_{vap}	Actual vapor pressure, [mm Hg]
P_{vap}^*	Saturated vapor pressure, [mm Hg]
Q	Volumetric flow rate i, [m^3/s]
q_i	Loading of component i, [kmole/kg SA9T]
q_w	Conductive heat transfer through wall, [kJ/(m^3·s)]
r	Radial spacial coordinate in cylindrical geometry, [m]
r_o	Inner radius of annulus, [m] -or- Toth isotherm parameter, [unitless]
r_f	Outer radius of annulus, [m]
R_e	Universal gas constant (energy units), 8.314472 [kJkmole^{-1}·K^{-1}]
R_g	Universal gas constant, 8.314472×10^{-2} [bar·m^3·kmole^{-1}·K^{-1}]
RH	Relative humidity fraction, [unitless]
SG	Specific gravity, [unitless]
T	Temperature, [K] -or- [°F]
t	Time, [s] -or- Toth isotherm parameter [unitless]

t_o	Toth isotherm parameter [unitless]
T_d	Dew point temperature, [°C] -or- [°F]
$\vec{v}$	Velocity vector, [m/s]
v	Velocity scalar, [m/s]
V_i	Volumetric flow rate of component i, [SLM]
y_i	Mole fraction of component i, [kmoles i/kmole]

Greek Letters

α	Freundlich isotherm parameter, [unitless]
ϵ	Void fraction, [unitless]
μ	Viscosity, [Pa·s]
ρ_s	Bulk density of sorbent pellets, [kg/m^3]

Superscripts & Subscripts

d	Downstream
g	Associated with gas
l	Lower
u	Upper -or- upstream
w	Associated with a wall